Wideband Slot Array Antenna Fed by Open-ended Rectangular Waveguide at W-band

Liu, Peiye; Pedersen, Gert Frølund; Zhang, Shuai

Published in:
I E E E Antennas and Wireless Propagation Letters

DOI (link to publication from Publisher):
10.1109/LAWP.2022.3140700

Publication date:
2022

Document Version
Accepted author manuscript, peer reviewed version

Wideband Slot Array Antenna Fed by Open-ended Rectangular Waveguide at W-band

Peiye Liu, Gert Frølund Pedersen, *Senior Member IEEE*, Shuai Zhang, *Senior Member IEEE*

***Abstract*—A wideband slot array antenna at W-band with a single-layer corporate feeding network is presented in this work. The radiating slots are fed by open-ended rectangular waveguides to widen the impedance bandwidth instead of a commonly used coupling mechanism. A subarray of two elements placed in the H-plane is designed. In order to fit the feeding network into one layer, a compact hybrid feeding network is used, which is a combination of ridge waveguides and E-plane hollow waveguides. An 8 by 8 elements array antenna is simulated and fabricated with brass. Two metal layers are assembled by the bottom edge of the ridge waveguide to minimize the power leakage through the gap. The measured prototype achieves a relative impedance bandwidth of 35.7% with a reflection coefficient below −10 dB from 77.5 to 111.2 GHz. A peak gain of 26.8 dBi with variations within 2.5 dB is obtained. The measured radiation patterns agree with the simulations quite well, and the gain reduction remains below 1 dB in the operating range.**

***Index Terms*—wideband, millimeter-wave, slot array antenna, single layer feeding network, hybrid feeding network.**

I. Introduction

Due to the growing demand for fast transmission rate and high capacity in the fifth-generation (5G) wireless communication system, wideband planner array antennas with high gain and low profile characteristics have attracted much interest [1]–[3]. W-band (75–110 GHz), with its low atmospheric absorption and wide usable spectrum bandwidth, which can offer gigabyte data transmission, has become a fascinating frequency range for such applications [4], [5].

The printed circuit board (PCB) based structures such as microstrip line or substrate integrated waveguide (SIW) [6], [7] are widely used in planar array antennas due to their flexibility in design. Some wideband applications have been reported [8]–[10]. However, the high dielectric losses significantly degrade the antenna gain when applied to large arrays at high frequencies. The same problem is with the low-temperature co-fired ceramic (LTCC) technology as reported in [11]. On the other hand, metal-based hollow waveguide structures with high gain and radiation efficiency characteristics attracted more attention. However, when it comes to millimeter-wave applications, the metal contact requirement between metallic layers is quite strict. The power leakage through gaps is not easy to avoid. Some methods have been introduced to minimize the leakage. In [12], [13], a fabrication method by the diffusion bonding of thin copper plates is reported. It effectively minimized the leakage at high frequencies. However, the method is costly, and the prototypes do not show impressive bandwidth. The 3D printing technology, which can realize the multi-layer structure in one piece, is applied in [14], [15]. In [16], a measured impedance bandwidth of 31% is achieved. However, the designs cannot be applied to W-band arrays, as the printing tolerance of 0.1 mm is unacceptable. The gap waveguide technology can depress the power leakage as it does not require electric contact between adjacent layers. As reported in [17], [18], around 30% relative bandwidth can be achieved. However, the periodic pin and multi-layer structures are bulky and complicated. Some other wideband designs also have been reported, such as continuous transverse stub array in [19] and E-plane waveguide fed array in [20]. However, these structures are too complex and have high fabrication accuracy requirements for W-band applications. Furthermore, all these wideband arrays mentioned above have at least two layers of feeding networks. The multi-layer structures make the designs bulky, high profiles, and complex in manufacture. Some single-layer designs have also been reported [21], [22], but the bandwidth is relatively narrow.

In this work, an 8 by 8 slots array antenna with a single-layer corporate feeding network is designed. The radiating slots are excited by open-ended rectangular waveguides to widen the impedance bandwidth instead of the commonly used coupling aperture mechanism. A compact hybrid feeding network that combines E-plane hollow waveguides and ridged waveguides is used, enabling the feeding network to be implemented into a single layer. Then the two pieces of the antenna are assembled by the bottom edge of the ridge waveguide to suppress the effect of the possible gap between layers. The proposed design is simple and stable in wideband applications for millimeter-wave array antennas.

II. Antenna Geometry

A. Antenna Array Geometry

The proposed antenna configuration is shown in Fig. 1. Slots with cavities on top are used as the radiating elements. Each slot is fed by a vertically placed rectangular waveguide from the bottom. A 1-to-64 way hybrid feeding network is implemented in the bottom layer. The transition from a standard waveguide WR-10 is placed at the back of the antenna as the feed port. The overall size of the antenna is $32 \times 32 \times 4\,\text{mm}^3$. 5 mm at each edge is reserved for positioning pins and screws. In this work, simulations are done using the CST Microwave Studio (CST). The material used in simulations is brass with

This work was supported by the Innovations Fonden Project of Reconfigurable Arrays for Next Generation Efficiency (RANGE). (Corresponding author: Shuai Zhang).

Peiye Liu, Gert Frølund Pedersen, and Shuai Zhang are with the Antennas, Propagation and Millimeter-wave Systems section at the Department of Electronic Systems, Aalborg University, Denmark (email: {liu,gfp,sz}@es.aau.dk).

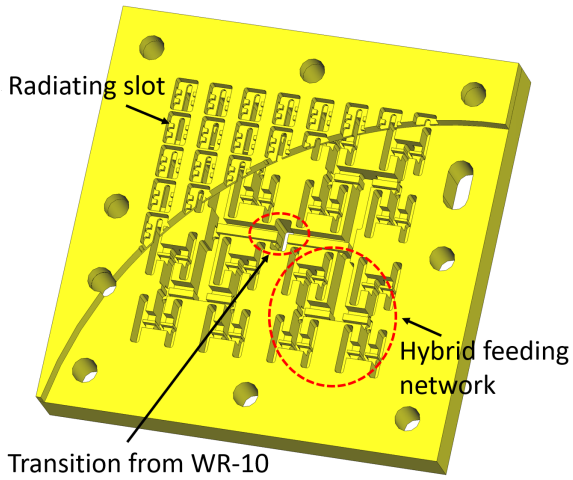

Fig. 1. Configuration of the proposed 8 by 8 slots array antenna.

a surface roughness of 0.0008 mm. Its electrical conductivity is set as 1.63×10^7 S/M.

B. Antenna Subarray

As mentioned above, most metal-based array antennas are designed with a double-layer structure with a 2 by 2 elements cavity fed by a coupling aperture below. It is mainly because the space to implement the one-to-one excitation is quite limited without dielectric material load. However, the configuration increases the complexity and profile of the antenna. Also, it limits the matching impedance bandwidth as the aperture coupling mechanism has a narrower bandwidth than open-ended rectangular waveguide fed.

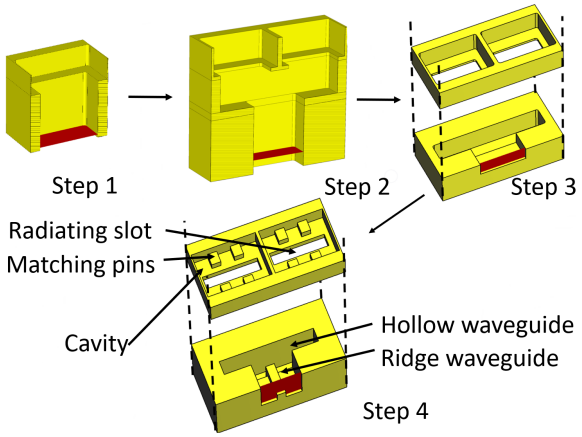

Fig. 2. The design process of the subarray (step 3 and 4 in the exploded view).

The design process of the subarray is depicted in Fig. 2. The first one is an open-ended waveguide with a cavity on top working as the unit cell. The second one is a subarray with 2 by 1 unit cells arranged in the H-plane with a vertical T-junction. To simplify the feeding network in one layer, the feeding branch of the T-junction is transformed horizontally as in step three. The final design of the subarray is shown in step four. A ridge waveguide replaces the horizontally arranged hollow waveguide to minimize its cross-sectional. Four pins are added on top of each slot to improve impedance matching. The optimized result is shown in Fig. 3. In the whole W-band, the reflection coefficient is below −15 dB. The element spacing is 2.75 mm, which corresponds to 84.8 % wavelength at the center frequency in free space. Other optimized parameters of the subarray are listed in Table I.

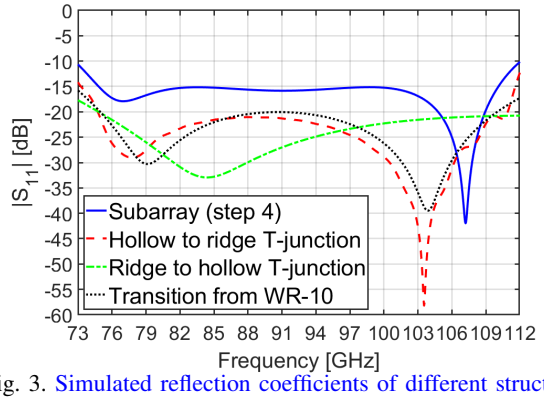

Fig. 3. Simulated reflection coefficients of different structures.

Table I. Optimized parameters of the subarray in Fig. 2 (step 4).

Paremeters	Width	Length	Height
Radiating slot	0.5mm	2.25mm	0.3mm
Cavity	1.85mm	2.62mm	0.85mm
Hollow waveguide	0.58mm	4mm	2.74mm
Ridge waveguide	1.73mm	1.08mm	1.75mm
Ridge	0.36mm	1.08mm	0.48mm
Matching pin	0.47mm	0.37mm	0.36mm
Distance between matching pins	0.55mm		

C. Feeding Network

To implement the feeding network into one layer, it has to be as compact as possible. In order to reduce the cross-sectional area, structures with E-plane T-junctions are employed in [2], [23]. However, its two output branches are 180° out of phase, which requires an extra bend structure to compensate. In this work, a hybrid feeding network constituted by E-plane hollow waveguides and ridge waveguides is implemented into a single layer. The hybrid structure was first proposed in [24] and applied in [22], [25]–[27] with gap waveguide technology. However, the structure is complicated and not suitable for mass production at W-band. The structures of hollow to ridge T-junction and ridge to hollow T-junction are shown in Fig. 4(a) and Fig. 4(b), respectively. The top metallic planes are hidden so the structures can be viewed. E-field distribution of the combined 4-way power divider is shown in Fig. 4(c). The ridge to hollow T-junction introduces the same phase in two output branches, while the outputs of the hollow to ridge T-junction have a 180° phase difference, which ensures the in-phase excitation of the slots. An iris and a stage are added inside the ridge to hollow T-junction for impedance matching. Furthermore, a transition section from the feed standard waveguide WR-10 to ridge waveguides is designed as

in [21]. The optimized reflection coefficients of hollow to ridge T-junction, ridge to hollow T-junction and transition section from WR-10 are depicted in Fig. 3. In the target frequency range from 75 to 110 GHz, $|S_{11}|$ is below −20 dB for all parts.

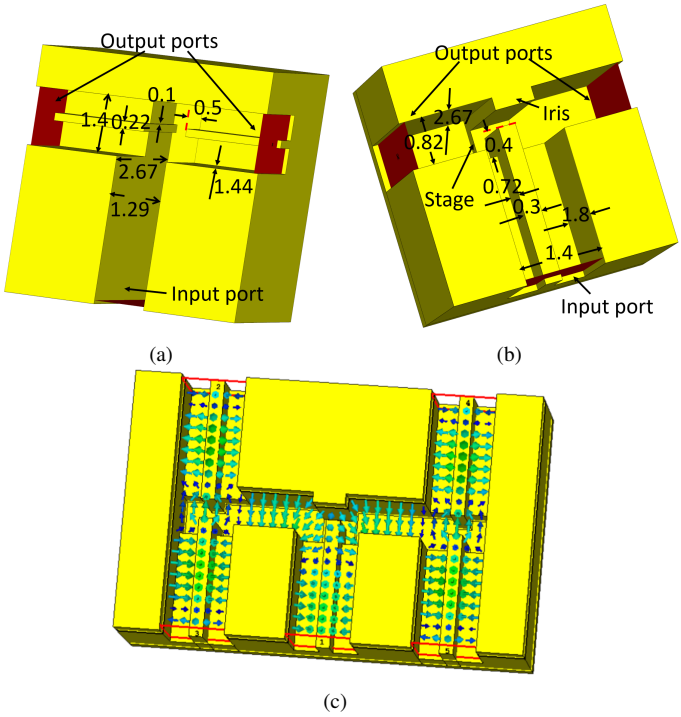

Fig. 4. The 3-D view of (a) hollow to ridge T-junction, (b) ridge to hollow T-junction, and (c) E-field distibution of combined 4-way power divider.

Finally, an 8 by 8 slots array antenna comprising subarrays and a 1 to 32 feeding network is re-optimized for impedance matching. All the shape corners are changed into fillets with a radius of 0.1 mm. In the final design, the minimum gap is above 0.2 mm. A new assemble method is introduced to minimize the leakage through the gap between layers. The ridge waveguides are assembled by the bottom edge of the sidewalls, as shown in Fig. 5. Sidewalls are on the backside of the top layer, while the ridges are on the bottom layer. In this way, the gap appears at the weakest position of the E-field inside ridge waveguides. Furthermore, power leakage of the E-plane hollow waveguides is also minimized, as it is cut almost in the middle where the current flow is minimum [20].

III. Measurements And Discussion

A prototype is fabricated with brass using computerized numerical control (CNC) machine. Material electrical conductivity is the same as in simulation. Surface roughness control is within 0.0008 mm. As shown in Fig. 5, the prototype is in two layers. The sidewalls of the ridge waveguide are hidden in the back of layer one. The other half of the feeding networks with ridges are milled on layer two. An extra adapter is used to connect the prototype with the mixer. The prototype is assembled using eight screws around the edges. The measurement is done in the anechoic chamber at the Antennas, Propagation, and Millimeter-wave Systems laboratory at Aalborg University.

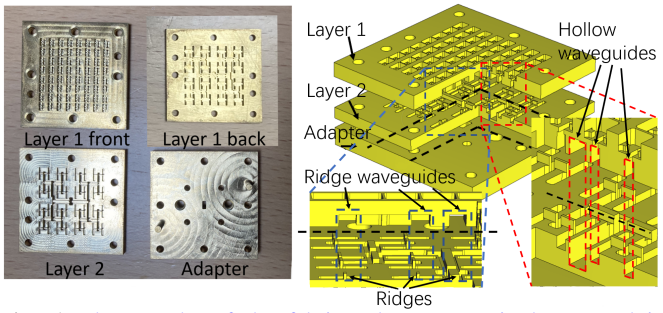

Fig. 5. Photographs of the fabricated prototype in layers and its assembling method.

As shown in Fig. 6, the impedance bandwidth for $|S_{11}|$ below −10 dB are 37.4% (from 74.4 to 108.6 GHz) and 35.7% (from 77.5 to 111.2 GHz), for simulation and measurement respectively. The measured results have some distortions and shift to a higher frequency range, mainly caused by the fabrication tolerance and assembling misalignment.

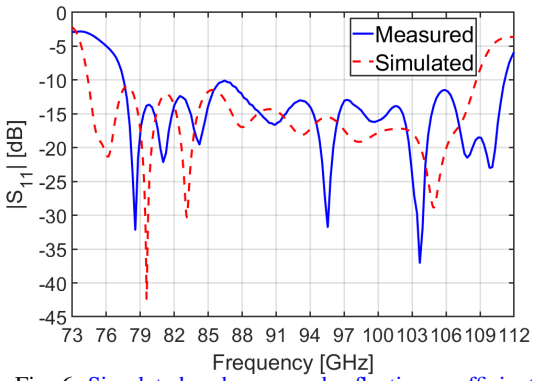

Fig. 6. Simulated and measured reflection coefficients.

The measured co-polarization and cross-polarization radiation patterns are compared with the simulations in Fig. 7. Due to facility limitations, frequencies above 110 GHz cannot be measured. It can be noted that the patterns are symmetrical and agree with the simulations quite well. The first sidelobe level is around −13 dB as the slots are excited uniformly. There are grating lobes that appear in the patterns of 110 GHz as the element spacing equals one wavelength. The cross-polarization level is below −32 dB in the whole operating band.

As shown in Fig. 8, the measured gain is over 24.3 dBi from 78 to 110 GHz, and reaches the max value of 26.8 dBi at 102 GHz. Compared with the simulation, the maximum gain reduction is only 1 dB at 86 GHz, which may due to fabrication tolerance, surface roughness, the small gap between the metal layers, and the measurement tolerance. The measured gain is close to the simulated gain. It can be confirmed that the power leakage through the gap is effectively minimized. As shown in Fig. 9, realized gains of different air gap sizes are simulated. Within 5 μm gap thickness, the gain drop is not significant. The chosen cutting plane does not significantly impact electric currents, and it can prevent field leakage. Similar to the measured reflection coefficient, a shift to the higher frequency range is observed. It is not available to measure directivity at our lab. The total efficiency is estimated using measured gain and simulated directivity. The radiation

Table II. Compared results between the proposed and reported wideband array antennas.

Ref.	Aperture size (λ_0^2)	No. of elements	Frequency (GHz)	Impedance bandwidth (−10 dB), (%)	Fabrication technology	No. of layers	Max. gain, (dBi)	Radiation Efficiency
Ref. [8]	5×5	8×8	37.5	31	PCB	4	23.5	77.8*
Ref. [11]	3×3	4×4	60	29	LTCC	5	17.5	80**
Ref. [16]	8×8	8×8	34	31	3D printing	1	28.5	89
Ref. [18]	6.73×5.96	8×8	59	30	Milling	3	27.5	80
Ref. [19]	12.66×6.93	16×1	33	42	Milling	5	29.1	75
Ref. [20]	6×6	8×8	12.5	36.9	Milling	3	26.3	90
This work	6.8×6.8	8×8	94	35.7	Milling	2	26.8	70

*Peak efficiency. ** Simulated efficiency.

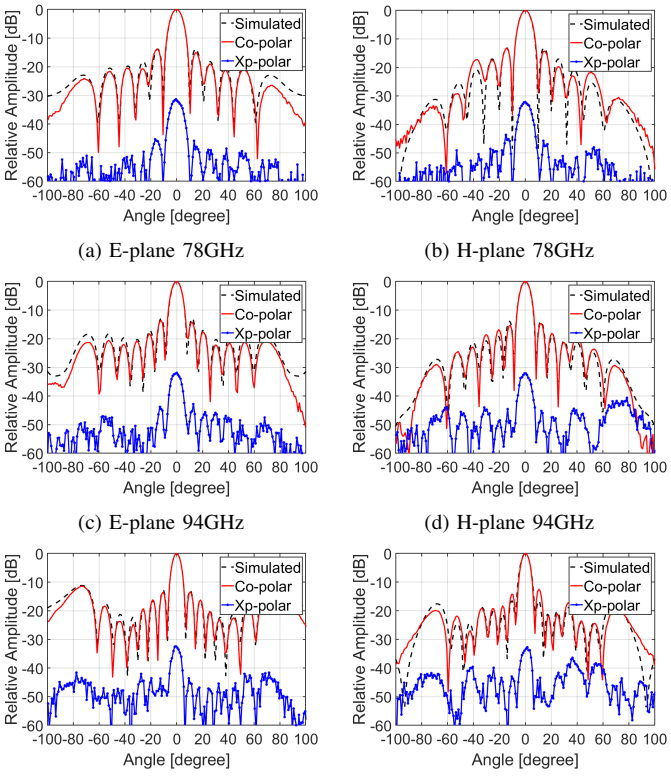

(a) E-plane 78GHz (b) H-plane 78GHz

(c) E-plane 94GHz (d) H-plane 94GHz

(e) E-plane 110GHz (f) H-plane 110GHz

Fig. 7. Measured co-polarization (Co-polar) and cross-polarization (Xp-polar) radiation patterns compared with simulated patterns.

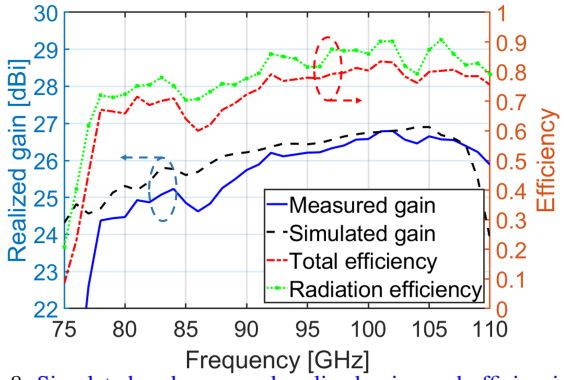

Fig. 8. Simulated and measured realized gains and efficiencies.

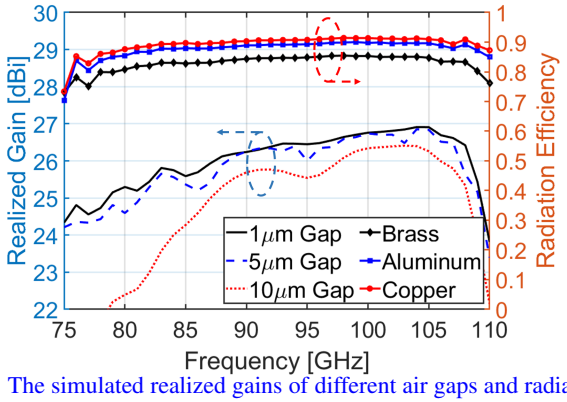

Fig. 9. The simulated realized gains of different air gaps and radiation efficiencies of different materials.

efficiency is estimated using estimated total efficiency and measured reflection coefficient. It varies from 70% to 90%. It is not outstanding compared with other reported prototypes. Because the material's electric conductivity is relatively low, and if any other material with high electric conductivity is used, such as copper or aluminum, the total efficiency can be much improved. As shown in Fig. 9, an average of 6% radiation efficiency can be improved from brass to copper when the mismatch factor is not considered.

Finally, the proposed structure is compared with various reported wideband array antennas, as shown in Table II. First, metal-based structures show big advantages in maximum gain than PCB [8] and LTCC [11]. Second, the proposed work has a much wider bandwidth than others except for [19], [20]. However, only this work achieves a two-layer structure, which can reduce fabrication workload and cost considerably. Although [16] can fabricate the sample in one piece, the low fabrication tolerance issue limits its application in W-band.

IV. Conclusion

An 8 by 8 slots array antenna fed by a compact hybrid feeding network in W-band is proposed in this work. The wideband performance is ensured by open-ended vertical waveguide fed slots. The single-layer hybrid feeding network significantly eases the fabrication complexity and cost. Moreover, its slicing method effectively prevents the gain deduction from power leakage through gaps at such high frequencies. The measured impedance bandwidth is 35.7% with $|S_{11}|$ below −10 dB. The prototype exhibits a realized gain of 24.3 to 26.8 dBi from 78 to 110 GHz. The proposed work shows good competitiveness in millimeter-wave wideband wireless communications with its simple structure and stable performance.

REFERENCES

[1] Z.-C. Hao, Q. Yuan, B.-W. Li, and G. Q. Luo, "Wideband *W*-band substrate-integrated waveguide magnetoelectric (ME) dipole array antenna," *IEEE Trans. Antennas Propag.*, vol. 66, no. 6, pp. 3195–3200, 2018.

[2] P. Liu, J. Liu, W. Hu, and X. Chen, "Hollow waveguide 32 × 32-slot array antenna covering 71–86 GHz band by the technology of a polyetherimide fabrication," *IEEE Antenna Wireless Propag. Lett.*, vol. 17, no. 9, pp. 1635–1638, 2018.

[3] X. Yi and H. Wong, "Wideband substrate integrated waveguide fed open slot antenna array," *IEEE Access*, vol. 8, pp. 74167–74174, 2020.

[4] N. Ghassemi, K. Wu, S. Claude, X. Zhang, and J. Bornemann, "Low-cost and high-efficient W-band substrate integrated waveguide antenna array made of printed circuit board process," *IEEE Trans. Antennas Propag.*, vol. 60, no. 3, pp. 1648–1653, 2012.

[5] C. R. C. Johnson, *Antenna Engineering Handbook, 3rd ed*. New York: McGraw-Hill, 1993.

[6] Y. Li and K.-M. Luk, "Low-cost high-gain and broadband substrate-integrated-waveguide-fed patch antenna array for 60 GHz band," *IEEE Trans. Antennas Propag.*, vol. 62, no. 11, pp. 5531–5538, 2014.

[7] Y. Li and K.-M. Luk, "60 GHz substrate integrated waveguide fed cavity-backed aperture-coupled microstrip patch antenna arrays," *IEEE Trans. Antennas Propag.*, vol. 63, no. 3, pp. 1075–1085, 2015.

[8] Q. Wu, J. Hirokawa, J. Yin, C. Yu, H. Wang, and W. Hong, "Millimeter-wave planar broadband circularly polarized antenna array using stacked curl elements," *IEEE Trans. Antennas Propag.*, vol. 65, no. 12, pp. 7052–7062, 2017.

[9] K. Ding and A. A. Kishk, "Multioctave bandwidth of parallel-feeding network based on impedance transformer concept," *IEEE Trans. Antennas Propag.*, vol. 67, no. 4, pp. 2803–2808, 2019.

[10] H. Xu, J. Zhou, K. Zhou, Q. Wu, Z. Yu, and W. Hong, "Planar wideband circularly polarized cavity-backed stacked patch antenna array for millimeter-wave applications," *IEEE Trans. Antennas Propag.*, vol. 66, no. 10, pp. 5170–5179, 2018.

[11] L. Wang, Y.-X. Guo, and W.-X. Sheng, "Wideband high-gain 60 GHz LTCC L-probe patch antenna array with a soft surface," *IEEE Trans. Antennas Propag.*, vol. 61, no. 4, pp. 1802–1809, 2013.

[12] Y. Miura, J. Hirokawa, M. Ando, Y. Shibuya, and G. Yoshida, "Double-layer full-corporate-feed hollow-waveguide slot array antenna in the 60 GHz band," *IEEE Trans. Antennas Propag.*, vol. 59, no. 8, pp. 2844–2851, 2011.

[13] D. Kim, J. Hirokawa, M. Ando, J. Takeuchi, and A. Hirata, "64 × 64-element and 32 × 32-element slot array antennas using double-layer hollow-waveguide corporate-feed in the 120 GHz band,," *IEEE Trans. Antennas Propag.*, vol. 62, no. 3, pp. 1507–1512, 2014.

[14] G.-L. Huang, S.-G. Zhou, T.-H. Chio, and T.-S. Yeo, "Fabrication of a high-efficiency waveguide antenna array via direct metal laser sintering," *IEEE Antenna Wireless Propag. Lett.*, vol. 15, pp. 622–625, 2016.

[15] Y. Li, L. Ge, J. Wang, S. Da, D. Cao, J. Wang, and Y. Liu, "3D printed high-gain wideband waveguide fed horn antenna arrays for millimeter-wave applications," *IEEE Trans. Antennas Propag.*, vol. 67, no. 5, pp. 2868–2877, 2019.

[16] Y. Li, L. Ge, J. Wang, B. Ai, M. Chen, Z. Zhang, and Z. Li, "A *Ka*-band 3D printed wideband stepped waveguide-fed magnetoelectric dipole antenna array," *IEEE Trans. Antennas Propag.*, vol. 68, no. 4, pp. 2724–2735, 2020.

[17] A. Farahbakhsh, D. Zarifi, and A. U. Zaman, "A wideband high-gain and high-efficiency slot array antenna based on groove gap waveguide," in *Proc. 12th Eur. Conf. Antennas Propag.*, pp. 1–3, 2018.

[18] A. Farahbakhsh, D. Zarifi, and A. U. Zaman, "A mmwave wideband slot array antenna based on ridge gap waveguide with 30% bandwidth," *IEEE Trans. Antennas Propag.*, vol. 66, no. 2, pp. 1008–1013, 2018.

[19] Q. You, Y. Lu, Y. You, Y. Wang, Z.-C. Hao, and J. Huang, "Wideband full-corporate-feed waveguide continuous transverse stub antenna array," *IEEE Access*, vol. 6, pp. 76673–76681, 2018.

[20] Z. Shi-Gang, H. Guan-Long, P. Zhao-hang, and L.-J. Ying, "A wideband full-corporate-feed waveguide slot planar array," *IEEE Trans. Antennas Propag.*, vol. 64, no. 5, pp. 1974–1978, 2016.

[21] J. Liu, A. Vosoogh, A. U. Zaman, and J. Yang, "A slot array antenna with single-layered corporate-feed based on ridge gap waveguide in the 60 GHz band," *IEEE Trans. Antennas Propag.*, vol. 67, no. 3, pp. 1650–1658, 2019.

[22] M. Ferrando-Rocher, A. Valero-Nogueira, J. I. Herranz-Herruzo, and J. Teniente, "60 GHz single-layer slot-array antenna fed by groove gap waveguide," *IEEE Antenna Wireless Propag. Lett.*, vol. 18, no. 5, pp. 846–850, 2019.

[23] P. Liu, G. F. Pedersen, and S. Zhang, "Wideband low sidelobe slot array antenna with compact tapering feeding network for E-Band wireless communications," *IEEE Trans. Antennas Propag.*, pp. 1–1, 2021.

[24] A. Jiménez Sáez, A. Valero-Nogueira, J. I. Herranz, and B. Bernardo, "Single-layer cavity-backed slot array fed by groove gap waveguide," *IEEE Antenna Wireless Propag. Lett.*, vol. 15, pp. 1402–1405, 2016.

[25] M. Ferrando-Rocher, J. I. Herranz-Herruzo, A. Valero-Nogueira, and A. Vila-Jiménez, "Single-layer circularly-polarized *Ka*-band antenna using gap waveguide technology," *IEEE Trans. Antennas Propag.*, vol. 66, no. 8, pp. 3837–3845, 2018.

[26] M. Ferrando-Rocher, J. I. Herranz-Herruzo, A. Valero-Nogueira, and B. Bernardo-Clemente, "Full-metal K-Ka dual-band shared-aperture array antenna fed by combined ridge-groove gap waveguide," *IEEE Antenna Wireless Propag. Lett.*, vol. 18, no. 7, pp. 1463–1467, 2019.

[27] M. Ferrando-Rocher, J. I. Herranz-Herruzo, A. Valero-Nogueira, B. Bernardo-Clemente, A. U. Zaman, and J. Yang, "8×8 *Ka*-band dual-polarized array antenna based on gap waveguide technology," *IEEE Trans. Antennas Propag.*, vol. 67, no. 7, pp. 4579–4588, 2019.